Synchronization properties of heterogeneous neuronal networks with mixed excitability type

Michael J. Leone,[1,2,*] Brandon N. Schurter,[3,*] Benjamin Letson,[4,5] Victoria Booth,[6]
Michal Zochowski,[7] and Christian G. Fink[8,†]

[1]*Mathematics Department, New College of Florida, Sarasota, Florida 34243, USA*
[2]*Program in Neural Computation, Carnegie Mellon University, Pittsburgh, Pennsylvania 15213, USA*
[3]*Physics Department, Berea College, Berea, Kentucky 40404, USA*
[4]*Mathematics Department, Ohio Wesleyan University, Delaware, Ohio 43015, USA*
[5]*Mathematics Department, University of Pittsburgh, Pittsburgh, Pennsylvania 15260, USA*
[6]*Mathematics Department and Anesthesiology Department, University of Michigan, Ann Arbor, Michigan 48109, USA*
[7]*Physics Department and Biophysics Program, University of Michigan, Ann Arbor, Michigan 48109, USA*
[8]*Physics Department and Neuroscience Program, Ohio Wesleyan University, Delaware, Ohio 43015, USA*

(Received 31 October 2014; published 30 March 2015)

We study the synchronization of neuronal networks with dynamical heterogeneity, showing that network structures with the same propensity for synchronization (as quantified by master stability function analysis) may develop dramatically different synchronization properties when heterogeneity is introduced with respect to neuronal excitability type. Specifically, we investigate networks composed of neurons with different types of phase response curves (PRCs), which characterize how oscillating neurons respond to excitatory perturbations. Neurons exhibiting type 1 PRC respond exclusively with phase advances, while neurons exhibiting type 2 PRC respond with either phase delays or phase advances, depending on when the perturbation occurs. We find that Watts-Strogatz small world networks transition to synchronization gradually as the proportion of type 2 neurons increases, whereas scale-free networks may transition gradually or rapidly, depending upon local correlations between node degree and excitability type. Random placement of type 2 neurons results in gradual transition to synchronization, whereas placement of type 2 neurons as hubs leads to a much more rapid transition, showing that type 2 hub cells easily "hijack" neuronal networks to synchronization. These results underscore the fact that the degree of synchronization observed in neuronal networks is determined by a complex interplay between network structure and the dynamical properties of individual neurons, indicating that efforts to recover structural connectivity from dynamical correlations must in general take both factors into account.

DOI: 10.1103/PhysRevE.91.032813 PACS number(s): 05.45.Xt, 87.19.lj, 87.19.ll

I. INTRODUCTION

Synchronization of neuronal networks is a prominent feature of brain activity, having been associated with directed attention [1,2], memory formation [3,4], and processing of sensory stimuli [5], as well as with pathologies such as Parkinson's disease [6] and epilepsy [7]. Results from nonlinear dynamical systems theory have been instrumental in understanding the factors which determine neuronal synchronization, which generally fall into two categories: dynamical properties of individual neurons and characteristics of the coupling structure between neurons.

Concerning the first category, most neurons exhibit one of two bifurcation structures in their transition to firing, saddle node, or Andronov-Hopf [8] (referred to as type 1 and type 2 excitability, respectively). Neurons exhibiting these two excitability types generally respond differently to brief perturbations [9], as characterized by the phase response curve (PRC). Assuming a periodically firing neuron, the PRC is a function which maps the phase at which a neuron is stimulated to the phase response of the neuron. Type 1 neurons usually exhibit phase advances (firing sooner than they would with no stimulus) for all stimulation phases, whereas type 2 neurons typically show phase delays at early stimulation phase and phase advances at relatively later stimulation phase. These qualitatively different responses to stimulation lead to dramatically different synchronization properties, with networks of type 2 neurons synchronizing much better than networks of type 1 neurons when coupled with excitation [10–12].

Considering the influence of coupling structure upon network synchronization, the master stability function (MSF) approach has proven a powerful tool for disentangling the effects of individual oscillator dynamics from network structure in contributing to a network's propensity for synchronization (PFS) [13]. MSF analysis has been applied to many network connectivity paradigms, including two which are commonly used to model connectivity within neuronal networks. The Watts-Strogatz (WS) small-world network model is useful because it interpolates between local, latticelike, and random connectivity structures using a single parameter, the rewiring probability p, which introduces "shortcuts" between nodes [14]. MSF analysis has shown that small-world PFS increases with increased number of shortcuts [15], increased network size, and increased connection density [16].

Scale-free (SF) networks, on the other hand, are characterized by a power-law degree distribution $p(k) \sim k^{-\gamma}$, a property that has been observed in the functional connectivity between hippocampal neurons *in situ* [17]. MSF analysis has shown that unweighted SF networks synchronize quite poorly in comparison with unweighted WS networks due to heterogeneity in degree distribution leading to hub nodes being

*These authors contributed equally to this work.
†cgfink@owu.edu

"overloaded" [18]. This poor PFS may be remedied, however, by weighting the incoming links to each node such that all nodes have the same total impinging connection strength. In this case, SF networks may synchronize as well as, or even better than, small-world networks [19].

While PRC theory and MSF theory have provided deep insight into the contributions of neuronal dynamics and connectivity structure to the synchronization of neuronal networks, there has been little investigation into the interplay between these two factors in networks that are heterogeneous with respect to excitability type. This may in part be due to the fact that classical MSF theory assumes a completely homogeneous network with respect to oscillator dynamics (although extensions to nearly identical oscillator dynamics have been made [20,21]). In this study, we numerically explore instances of two different network connectivity models, WS and SF, which have the same PFS according to MSF theory. We show that when the neuronal networks are homogeneous with respect to excitability type, either all type 1 or all type 2, both connectivity models exhibit the same degree of synchronization, consistent with calculations made using MSF theory. When dynamical heterogeneity is introduced, however, the synchronization properties of WS and SF networks can be either similar or dramatically different, depending upon correlations between node degree and excitability type. In particular, setting the hub nodes in SF networks to type 2 excitability results in a dramatic increase in synchronization compared to WS networks with the same proportion of type 2 neurons.

II. NEURON MODEL

For our numerical investigation of mixed-excitability-type networks, we used the Morris-Lecar (ML) model neuron, which is governed by the following equations:

$$C\frac{dV_i}{dt} = -g_{Ca}m_\infty(V_i)(V_i - E_{Ca}) - g_K w_i(V_i - E_K) - g_L(V_i - E_L) + I_i^{\text{syn}} + I_i^{\text{ext}}, \quad (1)$$

$$\frac{dw_i}{dt} = \phi\frac{w_\infty(V_i) - w_i}{\tau_w(V_i)}, \quad (2)$$

$$m_\infty(V_i) = \frac{1}{2}\left[1 + \tanh\left(\frac{V_i - V_1}{V_2}\right)\right], \quad (3)$$

$$w_\infty(V_i) = \frac{1}{2}\left[1 + \tanh\left(\frac{V_i - V_3}{V_4}\right)\right], \quad (4)$$

$$\tau_w(V_i) = 1/\cosh\left(\frac{V_i - V_3}{2V_4}\right), \quad (5)$$

where V_i is the membrane potential of the ith neuron, w_i is the corresponding recovery variable, I_i^{ext} is a constant external current, and I_i^{syn} is the synaptic current to neuron i induced by the firing of neurons coupled to neuron i. Parameter values are given in Table I, with modulation of the single parameter V_3 switching between type I and type II neuronal excitability [22,23]. Values of I_i^{ext} were uniformly distributed over the interval [70.93, 76.65] μA/cm^2 for type 1 neurons and [76.06, 81.20] μA/cm^2 for type 2 neurons, corresponding to firing rates between 19.5 and 20.5 Hz in both cases.

TABLE I. Parameters for Morris-Lecar model neurons, from [22,23]. Switching the parameter V_3 from 12.0 to 2.0 mV switches the neuronal excitability from type 1 to type 2.

C	20 μF/cm^2
g_{Ca}	4.0 mS/cm^2
g_K	8.0 mS/cm^2
g_L	2.0 mS/cm^2
E_{Ca}	120.0 mV
E_K	−80.0 mV
E_L	−60.0 mV
V_1	−1.2 mV
V_2	18.0 mV
V_3	12.0 mV or 2.0 mV
V_4	17.4 mV
ϕ	1/15

Figure 1(a) shows the frequency-current curves for these two neuronal types, with the type 1 neuron firing at arbitrarily low frequencies and the type 2 neuron exhibiting a nonzero frequency threshold, typical of Andronov-Hopf bifurcations. The similarity between these two curves makes this particular parameter set attractive for network simulations since it largely controls for different frequency response between the two excitability types. Figure 1(b) shows PRCs at firing threshold for the two neuronal types, with the type 1 neuron showing an exclusively positive curve and the type 2 neuron featuring an early phase delay region and rightward skew, both features

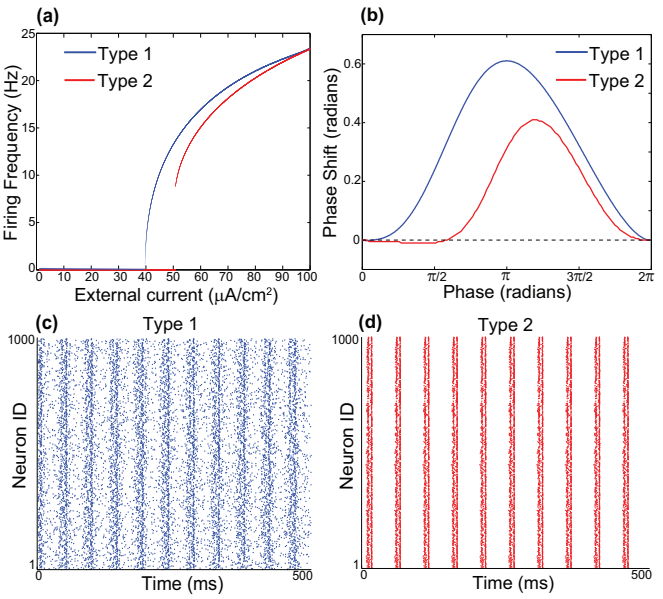

FIG. 1. (Color online) Characteristics of model neurons. (a) Frequency-current curves for Morris-Lecar neurons with type 1 (upper line) and type 2 (lower line) excitability. (b) Phase response curves for type 1 (upper line) and type 2 (lower line) model neurons. (c), (d) Raster plots of network activity for homogeneous Watts-Strogatz small-world networks (with $p = 0.8$) composed entirely of either type 1 neurons (c) or type 2 neurons (d).

which have been shown to enhance synchronization under excitatory coupling [24–26].

In network simulations, neurons were conductance coupled with fast excitatory synapses, so that the synaptic current delivered from neuron j to neuron i due to a spike by neuron j at time t_j was given by

$$I_{ij}^{\text{syn}} = s_{ij} \exp\left(-\frac{t-t_j}{\tau}\right)(E_{\text{syn}} - V_i). \tag{6}$$

Fast excitation was modeled by setting $\tau = 0.5$ ms and $E_{\text{syn}} = 0$ mV. The total synaptic current to neuron i was simply $I_i^{\text{syn}} = \sum_{j\in\Gamma_i} I_{ij}^{\text{syn}}$, where Γ_i is the set of all neurons which synapsed onto neuron i. For both WS and SF simulations, coupling conductances s_{ij} were constrained such that the total coupling strength impinging on each neuron was the same throughout the network: $s_{ij} = \frac{S}{k_i^{\text{in}}}$ (where k_i^{in} denotes the in-degree of neuron i). This constraint is biophysically realistic in neuronal networks [27], and has been shown to enhance the PFS in SF networks to the point that it is comparable to the PFS observed in small-world networks [19]. Consistent with previous studies [10–12], homogeneous networks composed entirely of type 2 cells synchronized better than homogeneous type 1 networks for a wide range of values of the total synaptic strength S. Figures 1(c) and 1(d) show representative raster plots of network activity for $S = 14.0$ mS/cm^2, the coupling strength we used throughout this study.

III. NETWORK CONNECTIVITY

In order to investigate the interplay between connectivity structure and excitability type, we employed two fundamentally different network connectivity paradigms: Watts-Strogatz (WS) small-world networks and scale-free (SF) networks. In the WS model [14], each of N neurons sends outgoing connections to its nearest d neighbors, and with probability p each connection in the network is rewired to a randomly selected neuron. The rewiring parameter p thus interpolates between a latticelike, locally connected network and an essentially random network. We used Barabasi's preferential attachment model [28] to construct SF connectivity. Briefly, this model starts with a fully connected network of M neurons, and as additional nodes are introduced they each make c connections with previously established nodes, with the probability of connection being proportional to the degree of each node. Since Barabasi's protocol is for an undirected network, and neuronal networks are inherently directed, we randomly assigned directions to the connections resulting from the Barabasi algorithm. All networks in this study featured $N = 1000$ neurons and 4% connectivity.

We used MSF analysis to quantify the PFS of the model networks described above. MSF theory assumes a network of coupled, identical oscillators whose dynamics follow the general form

$$\dot{\mathbf{x}}_i = \mathbf{F}(\mathbf{x}_i) + S\sum_{j=1}^{N} \mathcal{G}_{ij}\mathbf{H}[\mathbf{x}_j], \tag{7}$$

where $\mathbf{x}_i$ is a vector representing the dynamical variables of the ith oscillator, $\mathbf{F}$ is a function governing the individual oscillator dynamics, and $\mathbf{H}$ is a linear vectorial function. $\mathcal{G}$ is a zero row-sum coupling matrix in which each diagonal element $\mathcal{G}_{ii}$ reflects the summed strength of all connections incoming to node i, $\mathcal{G}_{ii} = -\sum_{j\neq i}\mathcal{G}_{ij}$. It can be shown that the more compact the spectrum of eigenvalues of $\mathcal{G}$ is, the wider will be the range of parameters for which the synchronous state is stable [29]. For an undirected and symmetric network, this is most easily quantified using the ratio of the largest eigenvalue to the smallest nontrivial eigenvalue λ_N/λ_2, with smaller values implying better PFS [30]. For a directed network the eigenvalues are complex, but it can be shown that ordering the eigenvalues according to their real parts and taking the analogous ratio λ_N^r/λ_2^r is an appropriate measure of a directed network's PFS, so long as $\mathcal{G}$ meets the constraint $\sum_{j\neq i}\mathcal{G}_{ij} = 1$ for all i [31].

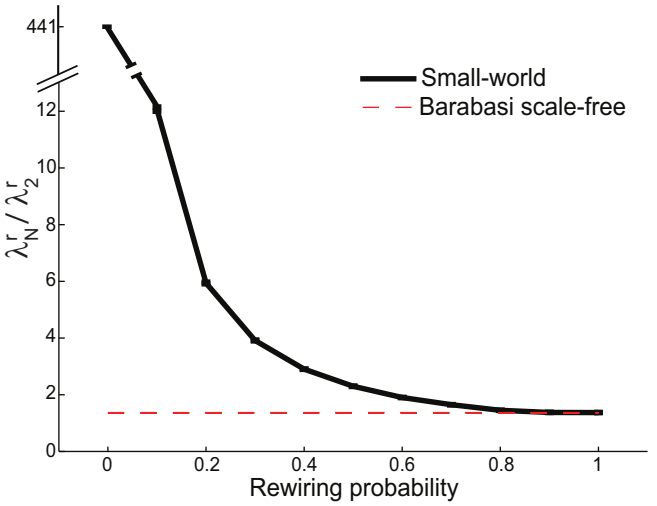

FIG. 2. (Color online) Propensity for synchronization of Watts-Strogatz and scale-free networks according to master stability function analysis. Each value plotted represents the average over 10 network realizations, with error bars representing s.e.m.

All WS and SF networks in this study met this constraint by construction, for we set $\mathcal{G}_{ij} = \frac{\mathcal{A}_{ij}}{k_i^{\text{in}}}$, where $\mathcal{A}$ is the network adjacency matrix (this also implies $s_{ij} = S\,\mathcal{G}_{ij}$). Normalizing the input to each cell in this way is biophysically realistic since manifold homeostatic plasticity mechanisms have been experimentally shown to prevent total synaptic input from growing too large or too small, thereby maintaining the stability of neuronal networks [27]. Figure 2 shows the PFS, as quantified by the ratio λ_N^r/λ_2^r, for WS networks as a function of the rewiring parameter p, as well as for the SF network model used in this study. Note how in terms of connectivity structure alone, SF networks have very nearly the same PFS as WS networks with $p \geqslant 0.8$.

IV. NETWORK SIMULATIONS

By comparing the synchronization of mixed-excitability $p = 0.8$ WS networks and SF networks, we were therefore able to investigate the effects of dynamical heterogeneity on network synchronization while controlling for the contribution of connectivity structure to network PFS. We ran a series of simulations of WS and SF networks in which the proportion of type 2 neurons comprising each network was varied

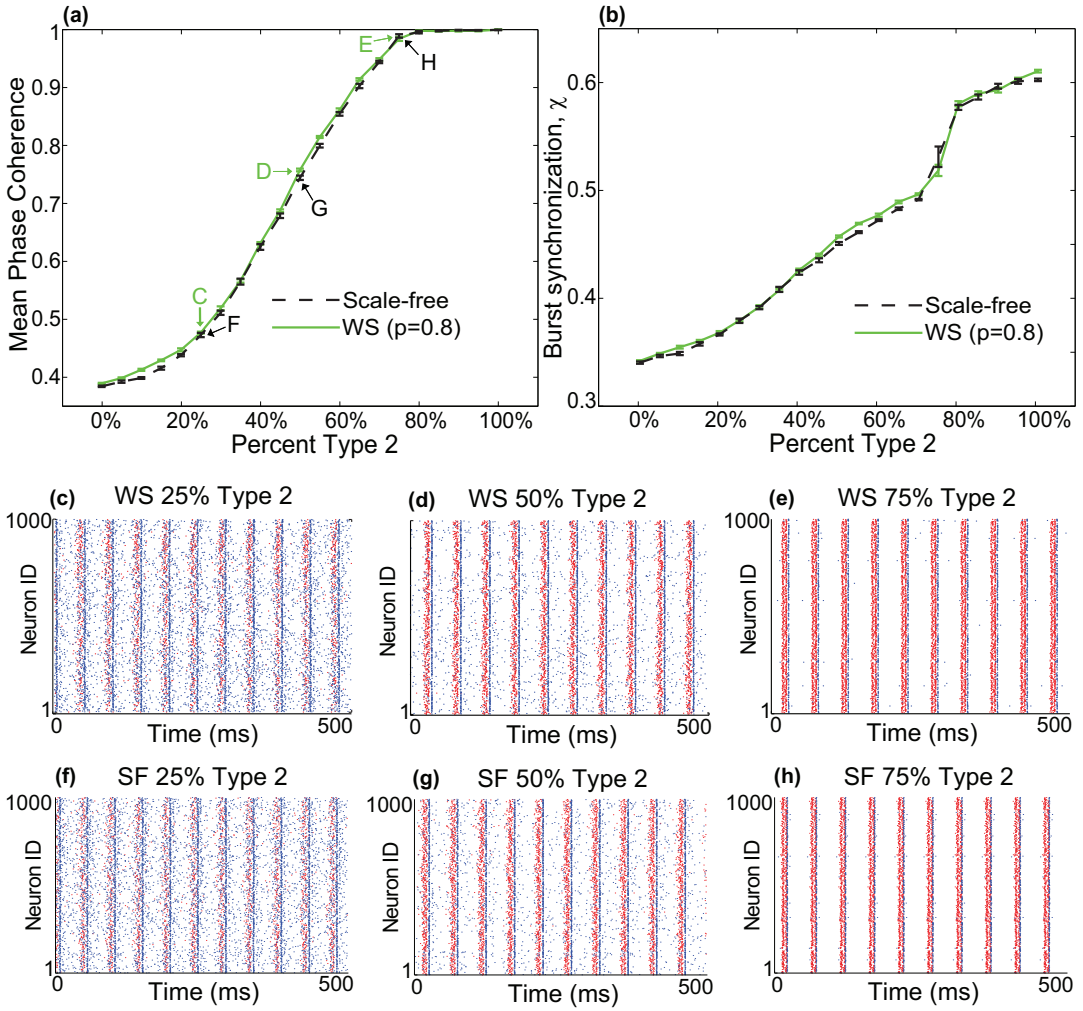

FIG. 3. (Color online) Effects of dynamical heterogeneity on the synchronization of SF and WS networks with random type 2 placement. (a) Phase-locking synchronization, as quantified by mean-phase coherence, as a function of percentage of type 2 cells present in SF and WS networks. Type 2 cells were placed randomly throughout both network types. (b) Measure of burst synchronization as a function of percentage of type 2 cells. (c)–(e) Raster plots depicting network spike times for networks with WS connectivity, for three levels of type 2 network composition. (f)-(h) Same as (c)–(e), but for networks with SF network connectivity. Blue (dark gray) dots indicate type 1 spikes, red (light gray) dots type 2 spikes.

(type 2 cells were randomly placed within each network). We then quantified both phase-locking synchronization and burst synchronization as a function of the fraction of type 2 neurons comprising the network. Briefly, phase-locking synchronization was quantified by averaging over the mean phase coherence (MPC) between all pairs of neurons [32], where MPC between two neurons was defined by

$$\sigma_{ab} = \left| \frac{1}{N_b} \sum_{k=1}^{N} e^{i\phi_k} \right|, \tag{8}$$

$$\phi_k = 2\pi \left(\frac{t_{b,k} - t_{a,k}}{t_{a,k+1} - t_{a,k}} \right), \tag{9}$$

where $t_{b,k}$ is the time of the kth spike of neuron b, $t_{a,k}$ is the time of the spike of neuron a that is largest while being less than $t_{b,k}$, $t_{a,k+1}$ is the time of the spike of neuron a that is smallest while being greater than or equal to $t_{b,k}$, and N_b is the number of spikes of neuron b. Burst synchronization χ was quantified using the measure of Golomb *et al.* [33]:

$$\chi^2 = \frac{\sigma_{\bar{V}}^2}{\frac{1}{N}\sum_{i=1}^{N} \sigma_{V_i}^2}, \tag{10}$$

where $\sigma_{\bar{V}}^2$ is the time-averaged variance of the mean voltage signal from all N neurons in the network, and $\sigma_{V_i}^2$ is the variance of just the ith voltage trace. This intuitive measure depends upon the increase in the variance of the mean voltage signal as bursting synchronization increases. Both MPC and χ are bounded on the interval [0,1], with MPC attaining a value of 1 when all neurons are perfectly phase locked, and χ attaining a value of 1 when all neurons continually fire together (or "burst") at exactly the same time.

Figures 3(a) and 3(b) show how these synchronization measures varied with proportion of type 2 cells present in the network. For both measures, synchronization of WS and SF networks increased monotonically with percentage of type 2 cells, and synchronization for the two connectivity paradigms

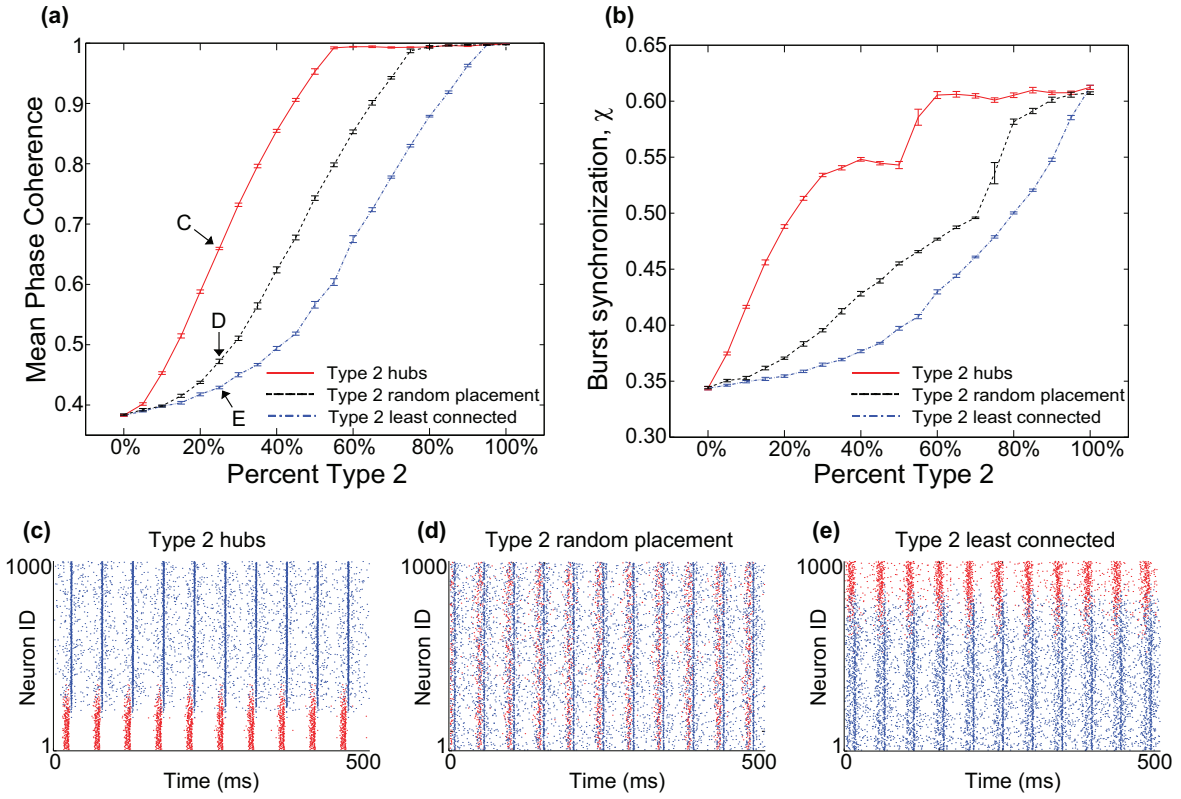

FIG. 4. (Color online) Effects of type 2 placement on the synchronization of SF networks. (a) Mean phase coherence of network activity as a function of proportion of type 2 cells composing the network, for three different type 2 placement procedures: (1) type 2 cells placed as the most highly connected cells, (2) random placement of type 2 cells, and (3) type 2 cells placed as the *least*-connected cells. (b) Bursting synchronization as a function of proportion of type 2 cells, with the type 2 placement procedures described in (a). (c)–(e) Raster plots depicting network activity for the three different placement procedures, with type 2 composition fixed at 25%. Blue (dark gray) dots indicate type 1 spikes, red (light gray) dots type 2 spikes. Note how when the most highly connected cells are type 2, they not only form their own cluster of elevated synchronization, but also increase synchronization throughout the rest of the network.

was virtually identical at the homogeneous extremes of either entirely type 1 or entirely type 2 network composition. This result accords well with the nearly identical PFS calculated for the two networks (Fig. 2) since MSF theory assumes homogeneous oscillator dynamics. More interesting is the nearly identical synchronization displayed by WS and SF networks for the various degrees of heterogeneity between these two extremes. For all values of type 2 percentage composition, WS and SF networks exhibited nearly identical phase locking and bursting synchronization. It should be noted that although Fig. 3 shows results for a rewiring parameter of $p = 0.8$ in WS networks, we also obtained nearly identical results using a value of $p = 1.0$ (data not shown).

Further investigation revealed that this effect was not generic, but depended upon the placement of type 2 cells within the network. Simulations of SF networks were conducted in which the placement of type 2 cells was correlated with the total degree ($k^{\text{in}} + k^{\text{out}}$) of each neuron, using three different placement procedures: for a given type 2 composition, (i) the most highly connected cells were switched from type 1 to type 2, (ii) the *least* highly connected cells were switched to type 2, and (iii) cells were randomly selected to be switched to type 2, irrespective of connectivity (as in Fig. 3). Figure 4 shows that these dynamical-structural correlations dramatically influenced network dynamics, with placement of type 2 cells as highly connected hubs leading to dramatically enhanced network synchronization. Compared to the least-connected and random placement procedures, placing type 2 cells as hubs resulted in network synchronization increasing much more rapidly as type 2 composition increased. This is clearly demonstrated in the raster plots of Figs. 4(c)–4(e), which show how type 2 hub cells not only formed a cluster of tight synchronization amongst themselves, but also recruited the remaining type 1 neurons to a higher level of synchronization than was observed when type 2 placement was uncorrelated or negatively correlated with neuronal degree.

In order to better investigate how type 2 hub cells were capable of "hijacking" type 1 cells to synchronization, we measured the mean phase coherence and burst synchronization of type 1 and type 2 populations separately, as a function of percent type 2 hub cells composing the network [Figs. 5(a) and 5(b)]. There was an interesting interval, from 20% to 50% type 2 composition, in which type 2 cells exhibited higher phase locking than type 1 cells, but type 1 cells showed better burst synchronization than type 2 cells. This indicated that type 2 cells were more consistent in their firing pattern from burst to burst, but that individual type 2 bursts were not as tightly synchronized as type 1 bursts. This phenomenon is clearly

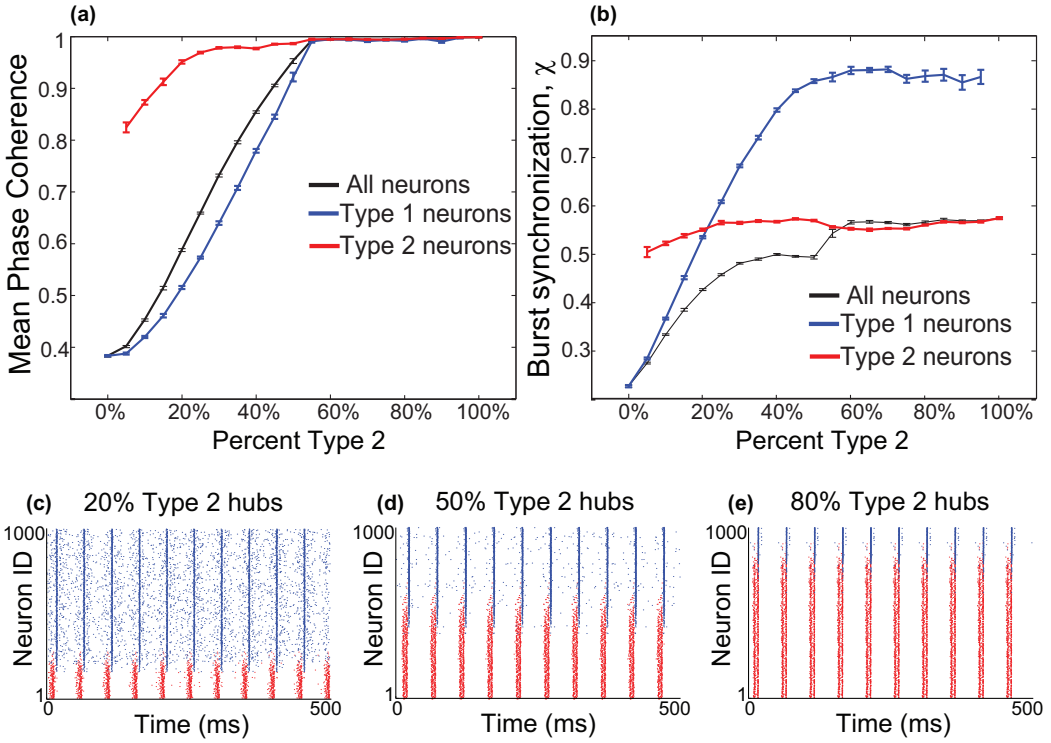

FIG. 5. (Color online) Synchronization of type 1 and type 2 populations of SF networks with type 2 hub cells. (a) Mean phase coherence of type 1 cells (lower line), type 2 cells (upper line), and all cells (middle line) as a function of type 2 network composition. (b) Burst synchronization of type 1, type 2, and all cells as a function of type 2 network composition (same color coding as in panel (a). (c)–(e) Raster plots of network activity for 20%, 50%, and 80% type 2 cells. Blue (dark gray) dots indicate type 1 spikes, red (light gray) dots type 2 spikes.

depicted in the raster plots of network activity [Figs. 5(c)–5(e)]. Also interesting was that with relatively few type 2 hub cells [Fig. 5(c)], peak type 1 burst activity lagged peak type 2 burst activity by ∼7 ms, but there were a sizable minority of type 1 cells that fired outside each type 1 burst.

We suspected that heterogeneity in the intrinsic firing frequencies of cells (which were distributed between 19.5 and 20.5 Hz across the network) was primarily responsible for both the imprecision of type 2 bursting and the large number of type 1 cells which seemed to randomly fire outside of type 1 bursts [Figs. 4(c) and 5(c)]. Simulations with homogeneous intrinsic frequencies (in which each cell naturally fired at exactly 20 Hz) did lead to much more precise type 2 bursting (Fig. 6), but, somewhat surprisingly, there were still a sizable minority of type 1 cells that did not fire with the majority of type 1 cells within each burst [Fig. 6(a)]. Moreover, we found that the type 1 cells that fired outside of the synchronous bursts was not consistent, but varied from burst to burst. This was especially surprising given the highly synchronous input received from the type 2 population.

Further investigation revealed that globally weakening all type 1 → type 1 coupling strengths led to a progressive decrease in the number of type 1 cells firing outside each network burst [Figs. 6(b)–6(d)]. With type 1 → type 1 coupling strengths reduced to 60% of their original value, all type 1 cells burst together. This seems to indicate that the synchronous "signal" received by type 1 cells from synchronous type 2 hub cells was somewhat drowned out by the "noise" from other type 1 cells when type 1 → type 1 coupling strength was high. Reducing type 1 → type 1 coupling strength would therefore enhance the signal-to-noise ratio, enabling bursts of type 2 hub cells to better drive type 1 network synchronization.

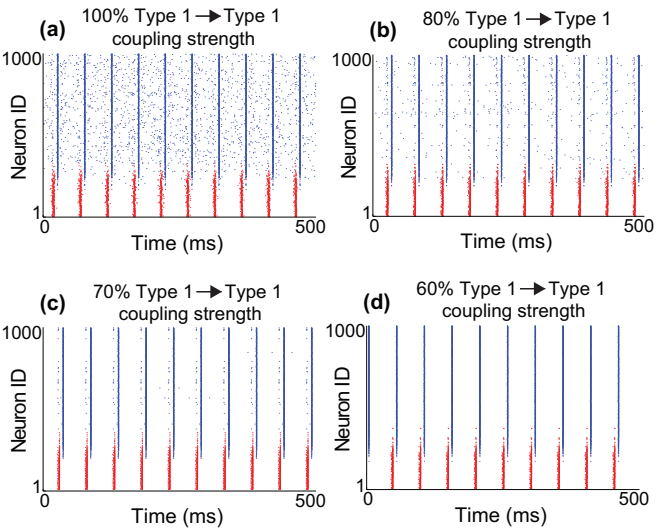

FIG. 6. (Color online) Effects of diminished type 1 → type 1 coupling strength on type 1 bursting. Simulations were run with exactly the same parameters as in Fig. 4(c), except that intrinsic cellular firing frequencies were homogenous (20 Hz) and type 1 → type 1 coupling strength was progressively decreased. (a)–(d) Fewer type 1 cells fired outside type 1 bursts as type 1 → type 1 coupling strength decreased. Blue (dark gray) dots indicate type 1 spikes, red (light gray) dots type 2 spikes.

V. DISCUSSION

Our results demonstrate that networks whose connectivity structures alone exhibit the same propensity for synchronization may nevertheless show dramatically different synchronization properties when local dynamical-structural correlations are taken into account. We have provided specific examples of two distinct network connectivity paradigms, WS small-world and scale-free, which have the same propensity for synchronization according to master stability function analysis, and show identical levels of synchronization for dynamically homogeneous networks, yet exhibit different synchronization properties for dynamically heterogeneous networks. Both types of networks show remarkably similar levels of synchronization for all type 1 and type 2 mixing ratios when type 2 cells are placed randomly, but their synchronization properties dramatically diverge when type 2 cells are placed either as hubs or as least-connected cells. (Analogous type 2 placement in WS small-world networks was not conducted because directed WS degree distribution is highly homogeneous.)

The dramatic influence of local dynamical-structural correlations on global network dynamics underscores the importance of taking these correlations into account when attempting to reconstruct network structure from measured dynamical correlations [34,35]. Furthermore, our results indicate that type 2 hub cells are exceptionally capable of "hijacking" neuronal networks to synchronization, while type 1 hub cells are not (Fig. 4). This may inform previous studies indicating that hub cells orchestrate network synchronization in the hippocampus [17] and contribute to epileptic seizures [36], suggesting that in some cases the hyperconnectedness of hub cells is not sufficient to orchestrate network synchronization, but must work in tandem with appropriate neuronal dynamics.

ACKNOWLEDGMENTS

M. Leone and B. Schurter were supported by National Science Foundation Grant No. 1003992. M. Zochowski was supported by NIH Grant No. NIBIB 1R01EB018297 and NSF Grant No. PoLS 1058034. V. Booth was supported by NSF Grant No. DMS-1121361.

[1] P. N. Steinmetz, A. Roy, P. Fitzgerald, S. Hsiao, K. Johnson, and E. Niebur, Nature (London) **404**, 187 (2000).
[2] P. Fries, J. H. Reynolds, A. E. Rorie, and R. Desimone, Science **291**, 1560 (2001).
[3] J. Fell, P. Klaver, K. Lehnertz, T. Grunwald, C. Schaller, C. E. Elger, and G. Fernández, Nat. Neurosci. **4**, 1259 (2001).
[4] U. Rutishauser, I. B. Ross, A. N. Mamelak, and E. M. Schuman, Nature (London) **464**, 903 (2010).
[5] A. K. Kreiter and W. Singer, J. Neurosci. **16**, 2381 (1996).
[6] R. Levy, W. D. Hutchison, A. M. Lozano, and J. O. Dostrovsky, J. Neurosci. **20**, 7766 (2000).
[7] P. Jiruska, M. de Curtis, J. G. Jefferys, C. A. Schevon, S. J. Schiff, and K. Schindler, J. Physiol. **591**, 787 (2013).
[8] E. M. Izhikevich, *Dynamical Systems in Neuroscience* (MIT Press, Boston, 2007).
[9] B. Ermentrout, Neural Comput. **8**, 979 (1996).
[10] S. Marella and G. B. Ermentrout, Phys. Rev. E **77**, 041918 (2008).
[11] S. Achuthan and C. C. Canavier, J. Neurosci. **29**, 5218 (2009).
[12] C. G. Fink, V. Booth, and M. Zochowski, PLoS Computat. Biol. **7**, e1002062 (2011).
[13] L. M. Pecora and T. L. Carroll, Phys. Rev. Lett. **80**, 2109 (1998).
[14] D. J. Watts and S. H. Strogatz, Nature (London) **393**, 440 (1998).
[15] M. Jalili, Chaos **19**, 033103 (2009).
[16] H. Fang, L. Qi-Shao, W. Marian, and J. Quan-Bao, Chin. Phys. B **18**, 482 (2009).
[17] P. Bonifazi, M. Goldin, M. A. Picardo, I. Jorquera, A. Cattani, G. Bianconi, A. Represa, Y. Ben-Ari, and R. Cossart, Science **326**, 1419 (2009).
[18] T. Nishikawa, A. E. Motter, Y.-C. Lai, and F. C. Hoppensteadt, Phys. Rev. Lett. **91**, 014101 (2003).
[19] A. E. Motter, C. Zhou, and J. Kurths, Phys. Rev. E **71**, 016116 (2005).
[20] J. G. Restrepo, E. Ott, and B. R. Hunt, Phys. Rev. Lett. **96**, 254103 (2006).
[21] J. Sun, E. M. Bollt, and T. Nishikawa, Europhys. Lett. **85**, 60011 (2009).
[22] K. Tsumoto, H. Kitajima, T. Yoshinaga, K. Aihara, and H. Kawakami, Neurocomputing **69**, 293 (2006).
[23] H. Kitajima and J. Kurths, Phys. A (Amsterdam) **388**, 4499 (2009).
[24] B. Ermentrout, M. Pascal, and B. Gutkin, Neural Comput. **13**, 1285 (2001).
[25] B. S. Gutkin, G. B. Ermentrout, and A. D. Reyes, J. Neurophysiol. **94**, 1623 (2005).
[26] B. Beverlin II, J. Kakalios, D. Nykamp, and T. I. Netoff, J. Comput. Neurosci. **33**, 41 (2012).
[27] G. G. Turrigiano and S. B. Nelson, Nat. Rev. Neurosci. **5**, 97 (2004).
[28] A.-L. Barabási and R. Albert, Science **286**, 509 (1999).
[29] S. Boccaletti, V. Latora, Y. Moreno, M. Chavez, and D.-U. Hwang, Phys. Rep. **424**, 175 (2006).
[30] A. Arenas, A. Díaz-Guilera, J. Kurths, Y. Moreno, and C. Zhou, Phys. Rep. **469**, 93 (2008).
[31] D.-U. Hwang, M. Chavez, A. Amann, and S. Boccaletti, Phys. Rev. Lett. **94**, 138701 (2005).
[32] F. Mormann, K. Lehnertz, P. David, and C. Elger, Phys. D (Amsterdam) **144**, 358 (2000).
[33] D. Golomb and J. Rinzel, Phys. Rev. E **48**, 4810 (1993).
[34] S. Feldt, P. Bonifazi, and R. Cossart, Trends Neurosci. **34**, 225 (2011).
[35] E. S. C. Ching, P.-Y. Lai, and C. Y. Leung, Phys. Rev. E **88**, 042817 (2013).
[36] R. J. Morgan and I. Soltesz, Proc. Natl. Acad. Sci. U. S. A. **105**, 6179 (2008).